CSUN

CSUN | CALIFORNIA STATE UNIVERSITY NORTHRIDGE

Final Report

The effect of power-line explosion on the performance of E-glass/Vinyl Ester Composite Panels Manufactured by Armorcast Products Co. for the Voltek System

Prepared by:

Dr. George Youssef

Assistant Professor of Mechanical Engineering and Director of the Experimental Mechanics Laboratory

Submitted to:

Armorcast Products Company

ARMORCAST

VOLTEK

VOLTEK VAULT REPLACEMENT SYSTEM

This report is submitted as part of cooperative agreement No. F-14-3575-1.0 between The University Corporation at California State University Northridge and The Voltek Division of Armorcast Products Company.

The effect of power-line explosion on the performance of E-Glass/Vinyl Ester Composite manufactured by Armorcast Products Co. for the Voltek System

George Youssef, *Ph.D.*
Mechanical Engineering Department – California State University Northridge

Background

Power surges in underground power vaults cause explosion, which in some cases results in fire hazards. Additionally, the explosion may possibly affect the structural integrity of the underground vault, which is currently constructed of reinforced concrete. The explosion has two possible byproduct loading scenarios on the vault. First due to conservation of energy, wire covers and splices can detach and act as projectiles that impact the side walls of the vaults, i.e. electrical energy due to power surge is converted to mechanical kinetic energy. Second, the fire creates localized increase in temperature on the surface, which may affect the physical properties of the vault materials. The impact loading and elevated temperature negatively affect the structural performance of steel reinforced concrete resulting in increased danger to the public.

Voltek International Inc. (a division of Armorcast Products Company) invented and patented a modular composite structure, VOLTEK® (US Patent No. US8413404-B2), to replace existing underground concrete vaults [1]. The advantages of Armorcast's Voltek System include, but are not limited to, ease of installation, minimum disruption of electricity and flow of traffic during installation, and the superior properties of composite materials. Nonetheless, in case of power surge induced explosion, the composite panels will be subjected to the same loading scenarios as in the case of concrete vaults, i.e. impact loading and elevated temperature. Impact loading gives rise to four possible major modes of failure in fiber-reinforced plastic (FRP) composites due to the heterogeneity and anisotropy of the materials [2-7]. Even at low velocity impacts, FRP can experience: 1) matrix failure mode due to tension, compression, or shear; 2) delamination of plies or at the skin/core interface due to inter-laminar stresses; 3) fiber breakage failure in tension or excessive buckling in compression; or 4) penetration of the impact projectile or damage [8]. The impact associated with power-line explosion can be classified as low velocity impact because of the panel's stiffness and materials properties are higher than the mass and stiffness of the impactor (detached objects). In other words, the response of the VOLTEK composite panels is dominated by its elastic behavior and not by the propagation of stress wave. Fire hazard from power-line

explosion increases the surface temperature of vault's panels and may cause an increase in the core temperature, which is dependent on the thermal conductivity of the FRP skin. Generally, the FRP skin has poor thermal conductivity properties due to the thermal properties of the polymer matrix [10-13]. The poor thermal properties of the skin is an added advantage in this case since it shields the wood core from any thermal loading. Additionally, the increase in temperature decreases the deformation resistance and degrades the polymer matrix, when subjected to repeated heating and cooling cycles. The latter depends on the microstructure, degree of crosslinking, degree of crystallinity, and type of polymer (i.e. thermoplastic or thermoset). For example, it was shown by Im et al. that the delamination areas of impact-induced damages decrease as temperature increases [12]. They also reported the delamination area per unit of impact energy decreased with increased surface temperatures [3, 12].

The mechanical behavior of polymers in general can be characterized using Dynamic Mechanical Analyzer (DMA), which is capable of reporting the material's properties as a function of temperature, frequency, environmental condition, or a combination of these parameters [17]. The DMA reveals information about major transitions as well as secondary and tertiary transitions not readily identifiable by other methods [18]. It allows characterization of bulk properties directly affecting material performance [18-27]. Figure 1 shows various molecular relaxations effects on the storage modulus as a function of temperature. The storage modulus is a measure of the materials resistance to deformation. The DMA has been previously used to study the effect of saline in the epoxy resin in composite materials and paint for marine applications [28], to find T_g and cure of composites, to determine α, β and γ relaxation of polymers, the calculation of activation energy, multi-frequency analysis of polymers, and influence of moisture and humidity on mechanical properties and T_g [29-31].

The objective of this project was to assess the modular composite vault panels by Armorcast Products Company before and after power surge induced explosion. The approach was to design and execute a series of material characterizations to qualitatively and quantitatively report on the effect of power-line explosion on the mechanical performance of the modular E-glass/Vinyl Ester panels and the extent of induced damage. The characterization techniques include: topographical

analysis using atomic force microscopy, cross-sectional damage analysis using optical microscopy, and mechanical testing using DMA.

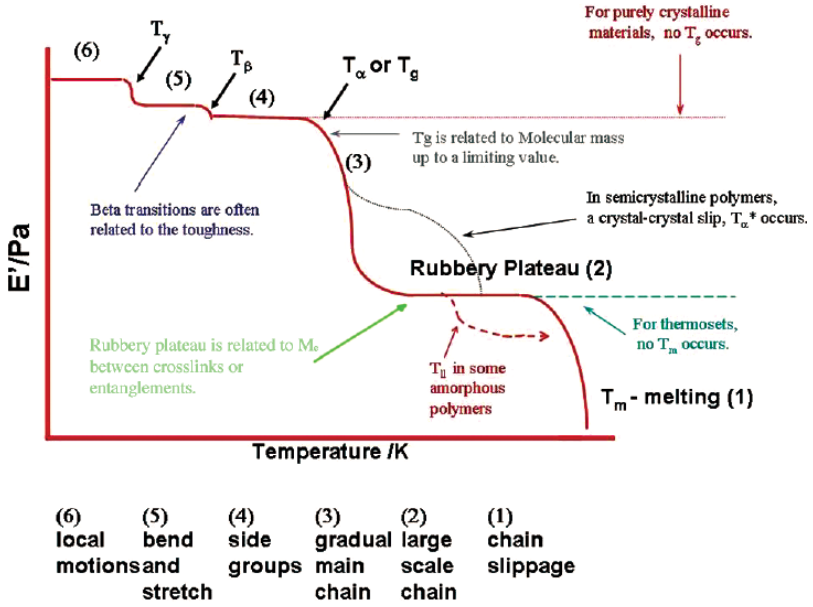

Figure 1: The effect of various molecular relaxations on the storage modulus [17].

Materials

The specimens used in this study were prepared from panels that were provided by Armorcast Product Company. The construction of all the panels was ~ 6.35 mm in skin thickness and ~ 140 mm in core thickness. Generally, the panel's skin is made of E-Glass/Vinyl Ester and the core is made of balsa wood [1]. Figure 2 shows the front view of the four sample blocks, which were harvested from field-deployed vault panels after a 34.5kVA power-line explosion [Exhibit 1]. The samples were extracted using ~152 mm dia. hole-saw from a vault located in Northridge, CA, and owned and operated by the Los Angeles Department of Water and Power (LA-DWP). The samples exhibit different degrees of contaminations and burn marks depending on the surrounding environment during installation, in-service conditions, and the proximity of the panels to the power-line explosion site, respectively. Figure 3 shows the profile view of the extracted samples, which indicates that the burn marks are limited to the surface and has not penetrated beyond few micrometers of the exposed surface. It is important to note that the balsa wood core did not show any signs of water absorption, which indicates that the E-glass/Vinyl Ester skin completely concealed the core from the surrounding environmental conditions. The burn mark shown on the profile view of the second sample block (Figure 3 – 2nd sample from the left) is attributed to the

extraction process, which resulted in burn marks on the wood core as the saw blade was cutting. In addition to these samples, Armorcast Products Company provided two completely new panels from the same product line, of which testing specimens were prepared. These panels were new off the production line and have not been deployed in the field. In short, specimens used in this experimental investigation were extracted from both field-deployed and new panels to compare the effect of field deployment, specifically power-line explosion, on the mechanical performance of the composite panels.

Figure 2: Front view of field harvested samples.

The specimens were prepared in two steps. In the first step, each sample block was cut into five rectangular slices using a band saw. Each slice was ~15 mm wide, ~70 mm long, and ~152 mm thick. These slices were used to investigate the bonding interface between the E-glass/Vinyl Ester skin and the balsa wood core by carefully examining the interface using optical microscopes. The wood core was also inspected under the microscope to uncover the effect of the power-line explosion on the wood fibers. In other words, if the panels experienced as excessively high impact loading, the wood fiber would buckle or break. Such failure would be easily observed using optical microscope. Another set of slices were cut from the new composite panel and underwent the same optical microscope investigations. This concluded the first step of the specimen preparation and investigation. In the second step, the wood core was completely removed using a band saw. The specimens were then polished using 100-grid sanding paper to completely remove the remaining wood. The wood core was removed before mechanical testing, given that the panels are expected to experience bending loading scenario under normal operating conditions and during impact

loading due to power-line explosion. In other words, the maximum tensile or compressive stresses is expected to be at the skin. Additionally, the length-to-depth ratio of the panel geometry is more than 10, which means that the transverse shearing effect can be neglected.

Figure 3: Side view of the field-harvested samples.

The final specimen size was ~12.7 mm wide, ~70 mm long, and ~6 mm thick samples. These specimens were used to measure the mechanical properties of the skin's materials using Dynamic Mechanical Analyzer (DMA) at specific testing conditions. The specimens were tested in dual-cantilever beam configuration, details of which are included in the next section. The DMA specimens were prepared from sample #3 (Figure 2 and 3) as well as from new composite panel to compare the mechanical performance of specimens from the worst-case affected panel to those of new panels.

Experimental Protocol

The experimental protocol was divided into three steps. First, investigation of surface, skin/core interface, and the wood fibers using an optical microscopy. Second, the surface topography of field-deployed and new specimens were characterized using Atomic Force Microscopy. The final step was measuring the dynamic mechanical properties of the specimens using DMA. Figure 4 shows a schematic that summarizes all the steps of the experimental protocol, the details of which are discussed next.

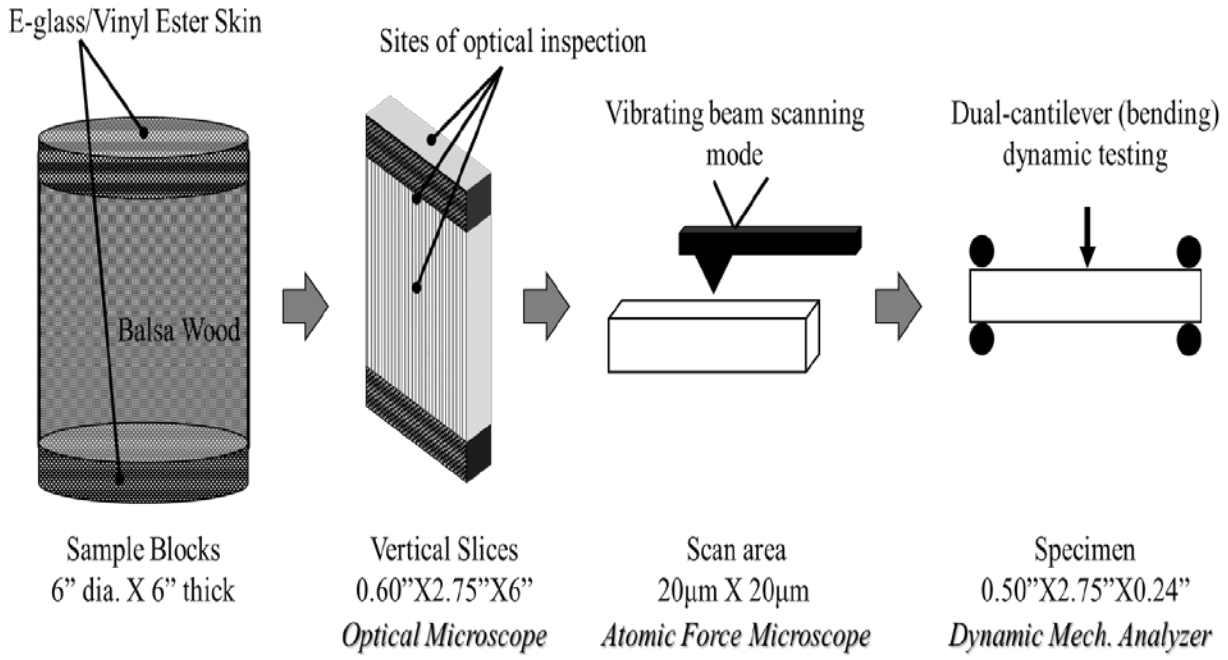

Figure 4: Schematic summary of the experimental protocol.

Optical Microscope

The impact loading scenario that is experienced by the composite panels during power-line explosion suggests four possible failure modes. These modes include inter-laminar failure, debonding at the core/skin interface, glass-fiber rupture, or wood-fiber failure. In addition, the thermal loading from the fire that accompanies the power-line explosion can cause surface or deep burns and excessive deformation due to the softening of the polymer matrix, if the temperature increases above the glass transition temperature. Vertical slices (Figure 4) of field-deployed and new samples were inspected under digital optical microscope (AmScope B490B-5M) at magnification of 10X in reflective mode using LED ring light (AmScope LED-2M-YA). The top surface of each specimen was first examined and then digital images were taken to document the evidence of burn marks, E-glass fiber breakage, or indentation due to excessive deformation. Thereafter, the cross-section of the specimen was carefully inspected for evidence of inter-laminar failure, debonding, wood-fiber failure, or matrix failure. Digital images were then studied and annotated using image processing software, some of which are included and discussed in the results section.

Atomic Force Microscope

The surface topography of each specimen was characterized using Atomic Force Microscope (AFMWORKSHOP SA-AFM). Specifically, 20µm X 20µm areas were scanned to determine the change in topographical features by the proximal interaction of a vibrating mechanical probe of the AFM with the surface of the specimen. All AFM scan runs were done in 3D mode at scan rate of 0.1Hz with resolution of 51.2 lines/micrometer and 25 samples/pixels. In each run, the amplitude and phase images were recorded and analyzed to understand the changes in surface stiffness or to detect any thermal transition due to the increase in temperature. Specimens cut from the new panels were scanned directly after removal of dust particles using compressed air, while specimens cut from field-deployed sample blocks were scanned after deep cleaning. The cleaning process was done to remove any surface contamination or residue (Figure 2 and 3). The specimens were cleaned in 50%-50% solution of distilled water and isopropyl alcohol in an ultrasonic cleaner for 1 hour. All AFM pictures were analyzed using Gwyddion scanning probe microscopy software.

Dynamic Mechanical Analyzer

To measure the dynamic properties of E-glass/Vinyl Ester skin materials, the specimens were tested using DMA (TA Instruments: Q800) in dual-cantilever beam configuration (Figure 5). The dual-cantilever beam configuration was selected because: 1) the skin material has high damping properties at and above the glass transition temperature (T_g); and 2) this configuration simulates actual loading scenario since the panels are clamped from all sides when installed in the field. The specimen geometry was calculated based on the geometrical factor (GF) of ~8.66 based on Equation 1. The GF is calculated to guarantee that the reported specimen moduli, i.e. storage and loss moduli, are not influence by the clamp stiffness.

$$GF = \frac{12l^3\left[1+\frac{12}{5}(1+\nu)\left(\frac{t}{l}\right)^2\right]}{24wt^3} \quad (1)$$

where, ***l*** is length of single arm of the dual-cantilever beam (35mm), ***t*** is the thickness of the specimen (~6mm), ***w*** is the width (~12.5mm), and ***v*** is the Poisson's ratio (taken to be 0.3 for calculation of GF).

Five specimens with width of 12.44±0.43 mm (95%) and thickness of 6.01±0.01 mm (95%) were cut from the field-deployed sample block that was most affected by the power-line explosion, i.e.,

sample block #3 in Figure 2, which exhibited the most burn marks and in-service contaminations of the supplied sample blocks. Additionally, four specimens 12.83±0.05 mm (95%) wide and 5.98±0.04 mm (95%) thick were extracted from the new composite panels. The length of the all the specimens was set to 70 mm, which was fixed by the distance between the stationary clamps (Figure 4).

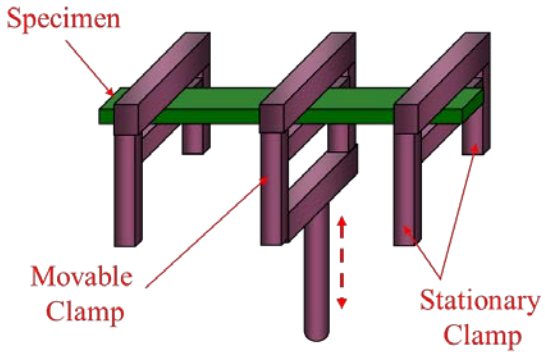

Figure 5: Schematics of dual-cantilever beam loading clamp in DMA.

As shown in Figure 5, the stationary clamps were fastened to the ends the specimens and the movable clamp fastened to the middle during mechanical testing. The bolts that held the specimens at these points were consistently torqued with 1.1N.m. pre-load for each run. At the beginning of the run, the temperature of the testing chamber was raised to 30°C and held constant for 20 minutes to allow the sample to reach thermal equilibrium while soaking at isothermal condition, i.e., constant temperature. Then, a force of 17N was applied at a frequency sweep of 5, 10, 20, 40 and 80Hz. The storage and loss moduli were calculated and recorded. The temperature was then increased by 10°C and the test was repeated until the temperature reached 210°C. Therefore, each run consisted of 18 different testing steps and lasted ~12 hours. The average moduli were calculated and the thermos-mechanical behavior of the materials was evaluated. The DMA testing procedure was based on ASTM D7264/D7264M-7 [34].

Results and discussion

Based on the results expected from the experimental protocol, discussed above, this section has been divided into two subsections: qualitative and quantitative. The optical microscope and the AFM results are included in the qualitative subsection, while the dynamic mechanical properties that were measured using DMA are included in the quantitative results subsection. The overall

objective of this section is to present the results and discuss the predicted implications of field deployment on the composite panels. It is important to note that the new panels were manufactured using the same process and materials as the field-deployed panels and thus the qualitative and quantitative comparisons are justified on these basis.

Qualitative Results

Figure 6 shows the surface micrographs of new E-glass/Vinyl Ester composite panels, which include six different digital images that were taken from different regions. All the images show consistent fiber/resin ratio and verify that the fibers are in tension regardless of the fiber orientation (Figure 6-a, 6-b, 6-d and 6-e). Figures 6-b and 6-f show small areas (note the scale on the right-lower corner of the image), where the matrix is not continuous and voids are present. The voids are attributed generally to the wet layup manufacturing process used to make the panels, where a relatively low viscosity resin is spread over the dry glass fiber and then pressed together in cold hydraulic press for curing. Finally, Figure 6-c shows entrapped bubbles on the surface, which are associated with the matrix curing process. That is, the matrix releases chemical volatiles as a byproduct of the curing process, which are inhibited from escaping due to the pressure applied by the cold-press to complete the curing.

Figure 6 shows twelve surface micrographs of the field-deployed panels that were exposed to in-service conditions and power-line explosion, as noted earlier. Similar to the new panel, these micrographs were taken from different surface regions from the most affected sample block (Sample #3 in Figure 2). Figure 7-a shows a clean portion of the surface, which indicates that although this region was in the vicinity of the explosion, i.e., adjacent to the regions in the remaining micrographs shown in the Figure 7, there is no significant change as it compares to pictures shown in Figure 6. Moreover, all the micrographs in Figure 7 resemble the characteristics of the new composite panel specimens as discussed in the previous paragraph. Specifically, the consistent fiber/resin ratio and fiber tension are evident, which are accredited to the consistency of the manufacturing process. The tension in glass fibers are clearly shown in Figures 7-d through 7-g, which indicates that surface temperature caused by the fire that accompanied the power-liner explosion never exceed the melting temperature of the matrix. The absence of evidence of fiber draping or embrittlement of the polymer matrix show that the surface temperature mostly likely

never exceeded the polymer softening temperature. In other words, the fibers remain in tension and the matrix remains without surface cracks.

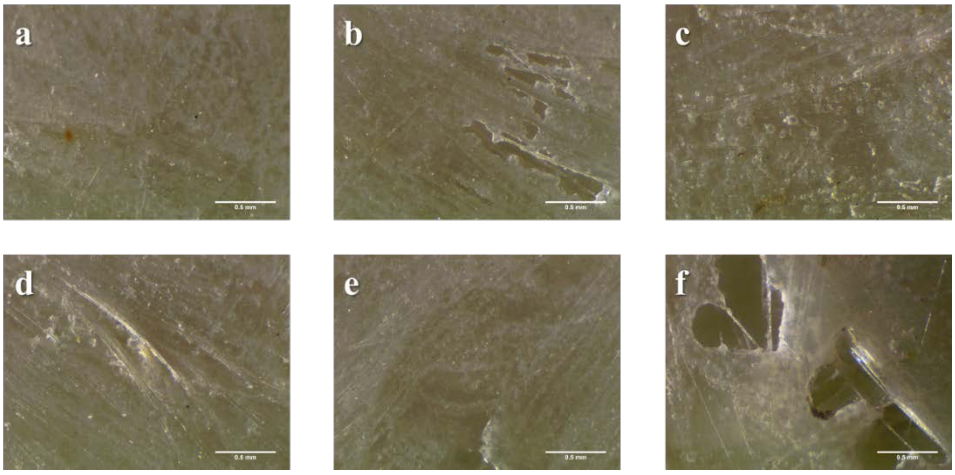

Figure 6: Optical micrographs of the surface of new (new) composite panels.

Figure 7-b through 7-f and 7-l show the presence of voids, which also attributed to the wet layup manufacturing process as discussed above. Also, the unaffected edges of the voids show that the voids existed before the power-line explosion and that the fire did not alter the materials in or surrounding the cavity of the voids. In the perspective of the entrapment of gaseous volatiles on the surface, Figures 7-c and 7-h show the existence of the bubbles on the surface covered by layers of contaminations of dusty (dull appearance) or oily (shiny and reflective appearance) natures. As discussed before, these bubbles are also a byproduct of the curing process and are not a result of in-service conditions.

The existence of surface contaminations due to installation or in-service conditions created a rich environment for the fire to affect the exposed surface of the composite panels. For example, Figure 7-k shows two adjacent regions on the same few millimeters-squared area, where the boundary of the highly-fire affected and mostly-unaffected, except for a slight color change (minor burn marks), regions is determined by the presence of surface contamination. The same effect can be observed on the remaining micrographs in Figure 7, where the existence of dust particles or surface contaminations left different level of burn marks compared to those on clean surfaces. Overall, the micrographs in Figure 7 show minor surface burn marks and an absence of excessive increase in the surface temperature, which is due to the fire-retardant properties of the composite panels. The

effect of temperature increase of the panels is investigated using AFM scans and will be discussed later in this report.

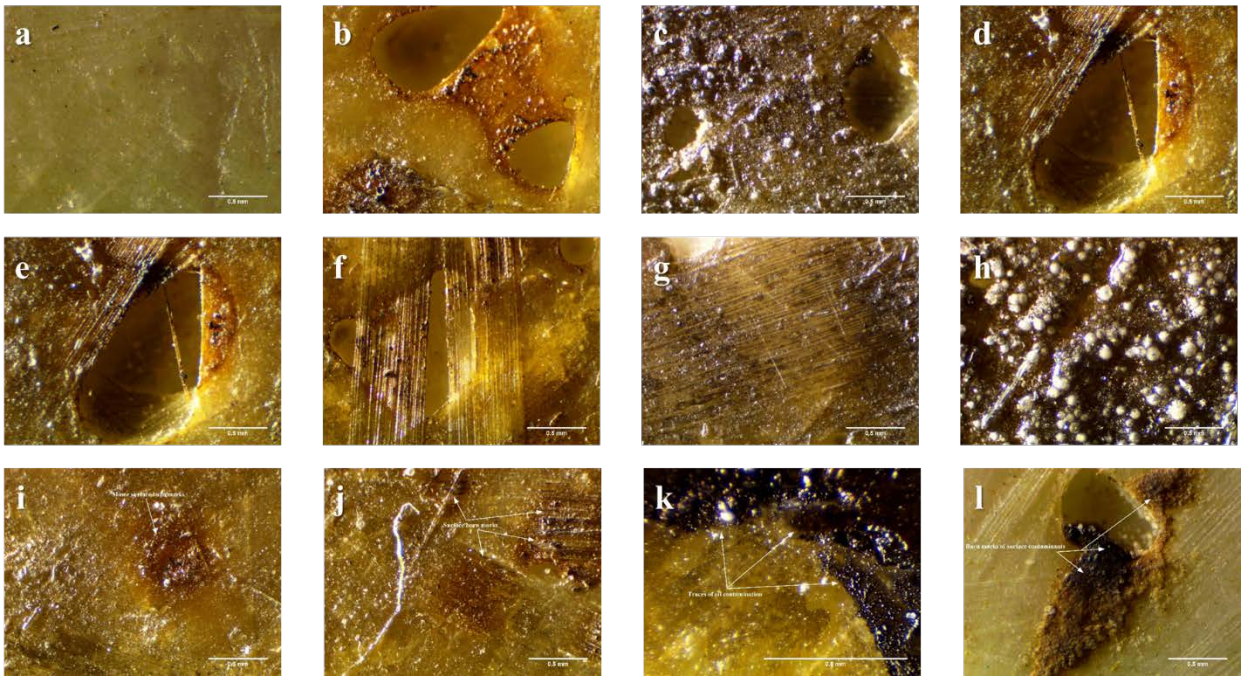

Figure 7: Optical micrographs of the surface of field-deployed samples after power-line explosion.

Figures 8 and 9 include series of digital images of the cross-section view of specimens cut from new and field-deployed panels, respectively. In analysis of these images, the focus was on explicating the nucleation of inter-laminar failure and the debonding of the skin/core interface that may have been caused by the power-line explosion or accompanied increase in temperature. When comparing Figures 8 and 9, it is evident that the composite panels remained unaffected by aforementioned harsh in-service conditions. The inter-laminar bonding strength and the skin/core bonding interface are higher than the mechanical and thermal stresses induced by the explosion and fire loading scenarios, respectively. This effect has been investigated using numerical simulation, the results of which are included at the end of this report.

The quantification of the bonding strengths are beyond the scope of this investigation but the survivability of the E-glass/Vinyl Ester composite panels has been shown to be superior except for the surface where surface contamination was present. Thus, based on the previously presented qualitative analysis of micrographs from new and field-deployed panels, it is advisable to ensure that the surface of the surface is clean, especially from oil contaminates.

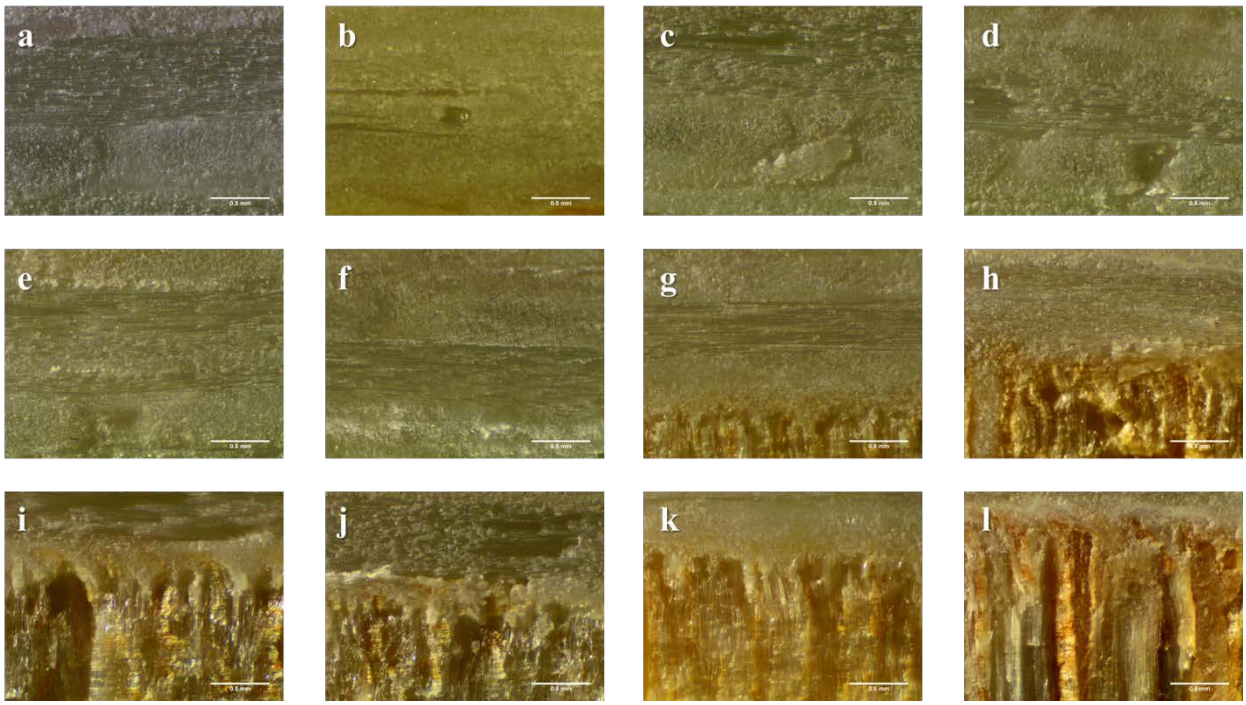

Figure 8: Cross-section images of new panels.

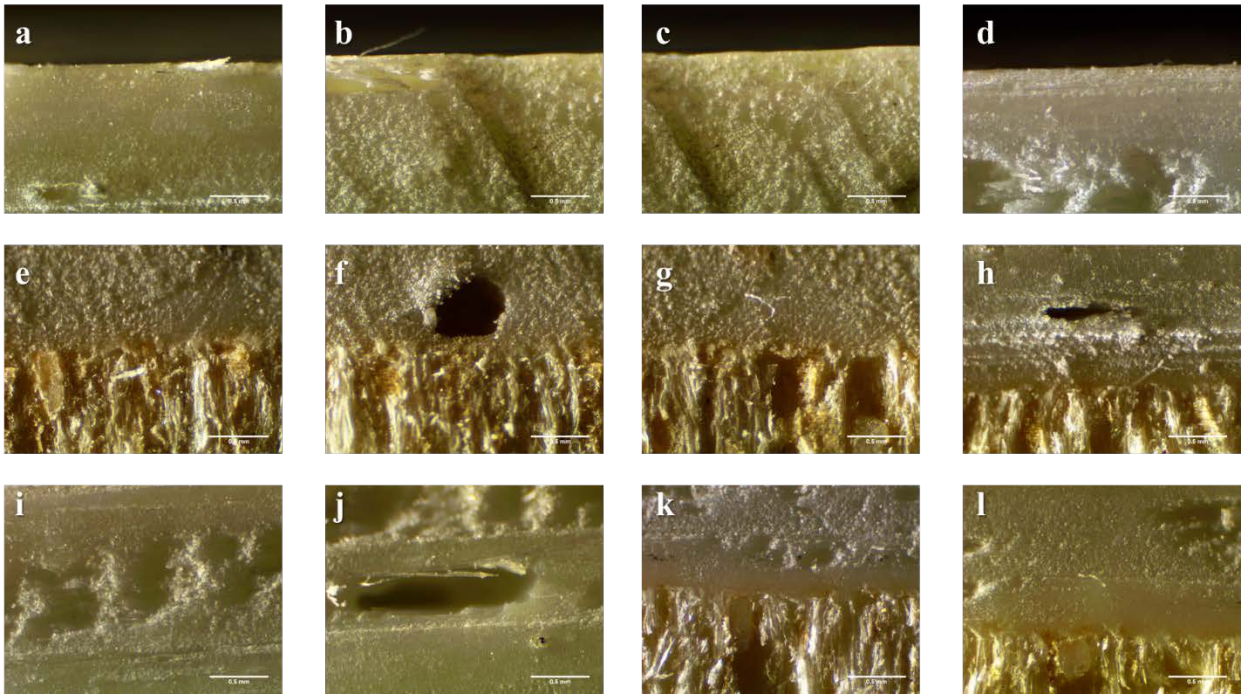

Figure 9: Optical images of the cross-section of field-deployed samples after power-line explosion.

The qualitative results of the Atomic Force Microscope scans are represented in the form of topography and phase images. The topography images elucidate the roughness of the surface,

while the phase images are representation of the force interaction between the scanning probe tip and the surface of the specimen. The AFM phase images have been shown to provide a map of stiffness variation of the specimen surface. Magonov et al. derived a relationship that correlates the phase shift ($\Delta\phi_o$) in AFM image to the surface stiffness, such that

$$\Delta\phi_o \approx \epsilon \bar{a} E^* \left(\frac{Q}{k}\right) \tag{2}$$

where, ϵ is a number between 1.9 and 2.4 based on Hertz theory, $\bar{a}$ is the average radius of the tip-specimen contact area, Q is the quality factor, k is the spring contact of the micro-tip, and the overall stiffness E_{eff} is defined as function of elastic moduli and Poisson's ratios of the tip (subscript t) and specimen (subscript s) [32-33]. Since the tip is considered to be much harder than the specimen, the overall stiffness is dominated by the specimen modulus as shown in Equation 3.

$$\frac{1}{E_{eff}} = \frac{(1-\nu_t^2)}{E_t} + \frac{(1-\nu_s^2)}{E_s} \tag{3}$$

That is to say, a stiffer region on an AFM phase image appears brighter than a softer or compliant region and thus the image contrast can be used to qualitatively investigate the change in stiffness due to in-service conditions.

Figures 10 and 11 show topography and phase of the surface from two different specimens that were cut from the new panel, while Figures 12 and 13 are the scans of specimens from field-deployed sample blocks. Generally, there is no significant change in the surface roughness, when comparing topographical images of new and field-deployed specimens. The aspect ratio of the surface roughness to the panel lateral dimension is very small. Therefore, it has a negligible effect on the overall mechanical performance of the composite panels in the field. Nonetheless, the contrast of the phase images from the new panels appears to be slightly darker than that from field-deployed samples. This represents change in the stiffness of the surface layer after the composite panels were exposed to harsh in-service conditions, e.g., surface contamination and power-line explosion. It is important to note here that the increase in the stiffness is only limited to the surface layer since optical images did not show any penetration of the burn marks into the thickness.

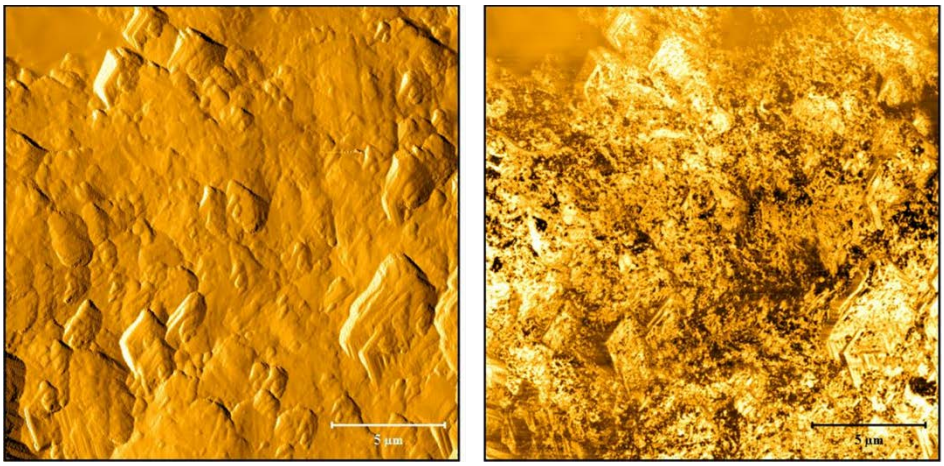

Figure 10: AFM topography (left) and phase (right) of specimen from new panel with scan size of 20µm X 20µm.

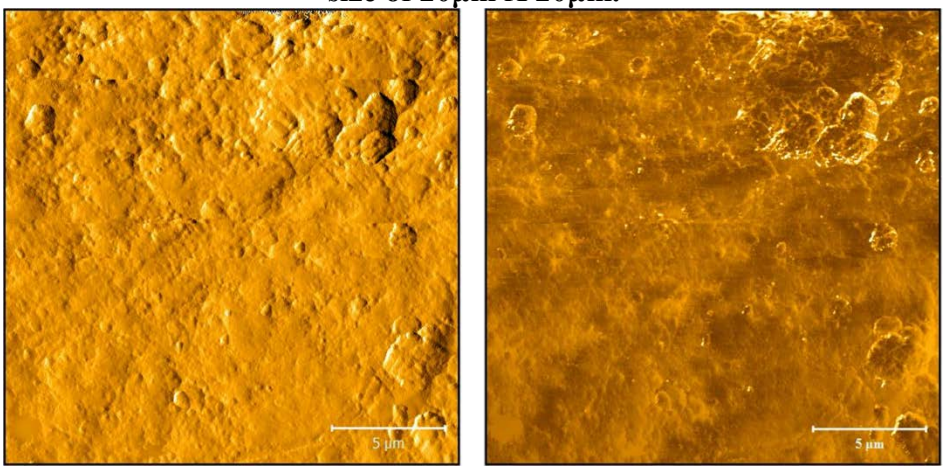

Figure 11: AFM topography (left) and phase (right) of specimen from new panel with scan size of 20µm X 20µm.

In Summary, the qualitative results supports the hypothesis of low velocity impact (low energy), which was discussed in the background section. Specifically, the absence of delamination, matrix damage, and fiber-failure, which are attributed to the lack of bending stiffness mismatch between adjacent plies, matrix cracks and matrix/fiber debonding were not observed, and low induced stress at the impact zone, respectively [8].

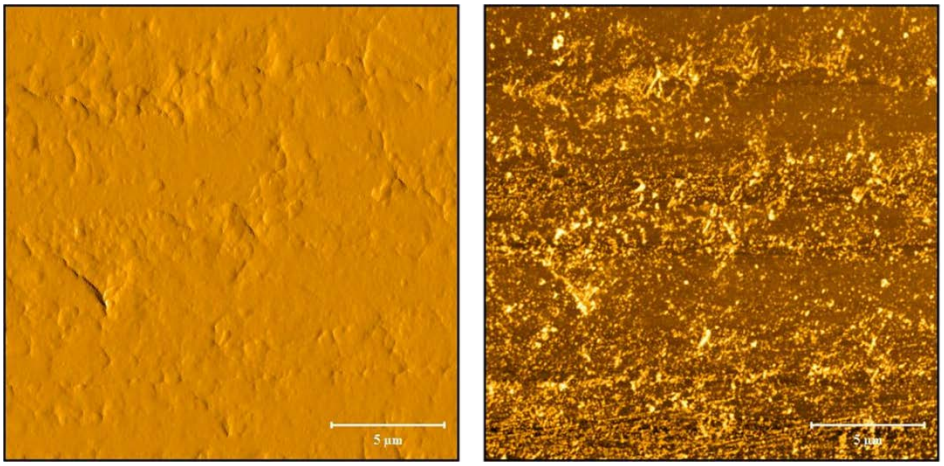

Figure 12: AFM topography (left) and phase (right) of specimen from field-deployed sample block with scan size of 20µm X 20µm.

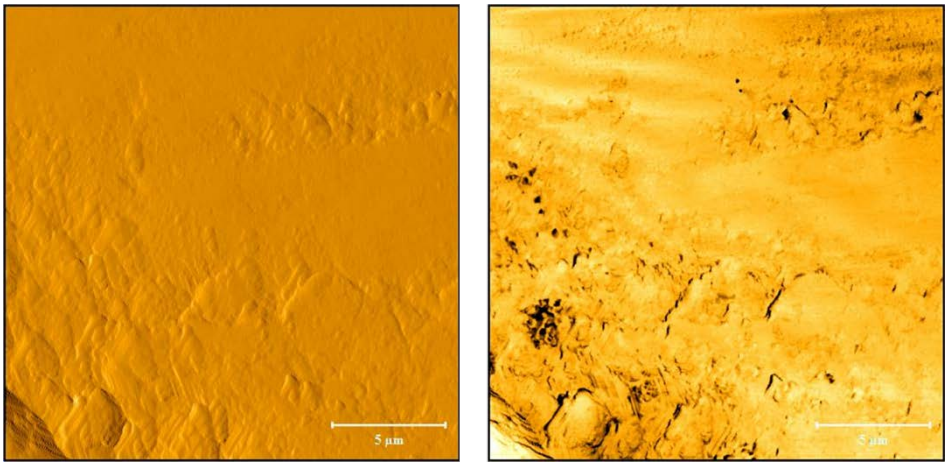

Figure 13: AFM topography (left) and phase (right) of specimen from field-deployed sample block with scan size of 20µm X 20µm.

Quantitative Results

Figures 14 and 15 show the thermo-mechanical spectra of the specimens cut from the new and field-deployed panels. The spectra is a plot of the storage modulus (E'), i.e., a measure of the laminate resistance to deformation, and the loss modulus (E"), i.e., a measure of the laminate energy dissipation or damping, as a function of temperature. As mentioned in the experimental protocol, the thermo-mechanical spectra were measured at different frequencies, the results of which are included in the figures below. In general, the spectra can be divided into three regions: the glassy regime, the leathery regime, and the rubbery regime. The glass transition temperature (T_g) defines the transition between the glassy and leathery regimes.

Figure 14 displays the average thermo-mechanical performance of four specimens from new panel. Below 100°C (~210°F), the laminate has flexural storage modulus of 9277±470 MPa and relatively low loss modulus, which is to say the laminate behaves as a quasi-isotropic and homogenous solid. The figure also shows two transition points, at which there is a noticeable drop in the storage modulus values. The first transition occurs at ~75°C, which is usually referred to as the beta transition (T_β) and related to change in toughness. T_β marks the transition between the matrix chains bending and stretching motion mechanism (below T_β) and sliding of chains (above T_β). The change in the molecular relaxation mechanisms results in increase in the area under the stress-strain curve; hence change in toughness. The T_β change is also observable as an increase in the loss modulus, which indicates an increase in the energy dissipation ability of the laminate. The second transition is the glass transition temperature (T_g), previously discussed before. Figure 14 also shows the dependency of T_g on the frequency, which varies from ~112°C at low frequency to ~120°C at high frequency.

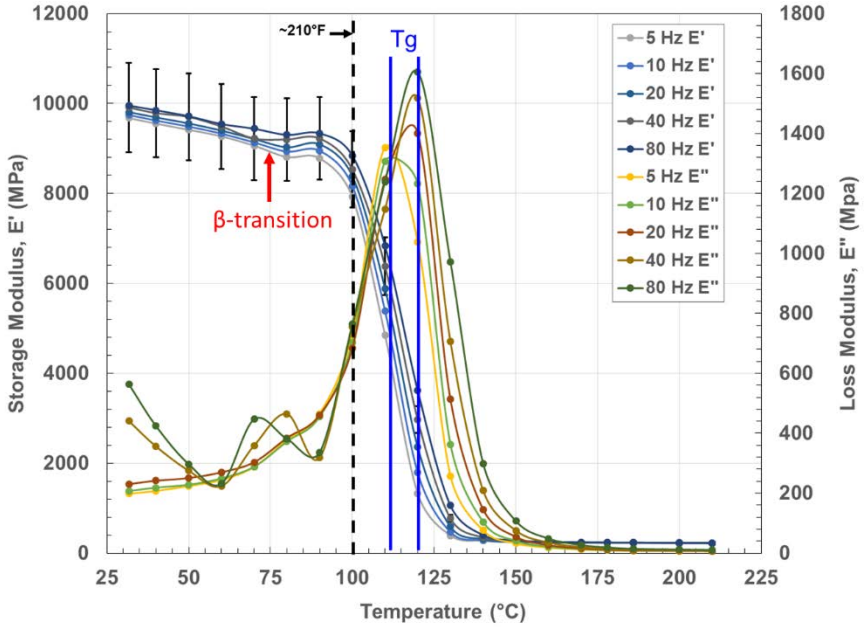

Figure 14: thermos-mechanical spectra of new specimen at different frequencies.

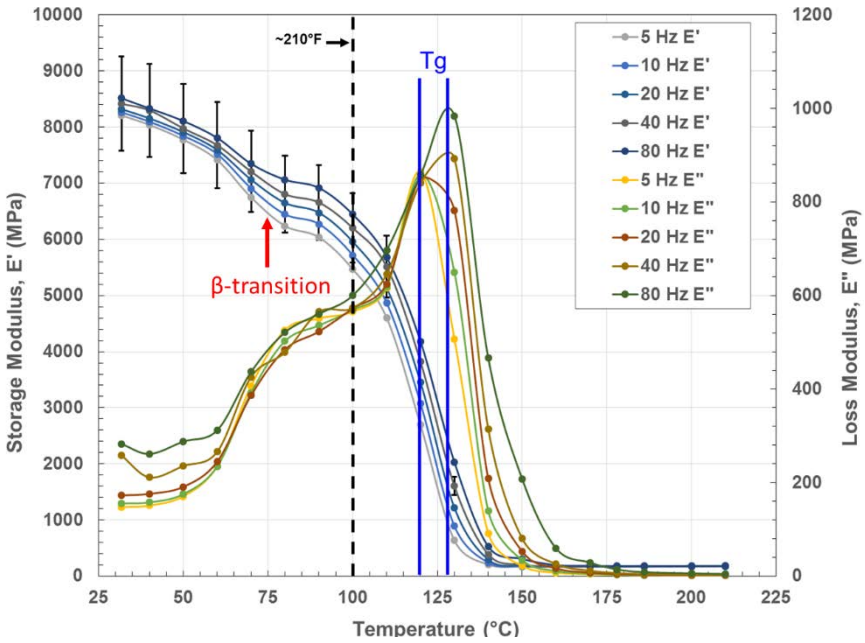

Figure 15: thermos-mechanical spectra of field-deployed specimen at different frequencies.

Similarly, Figure 15 displays the average thermo-mechanical behavior of five field-deployed specimens, where the storage modulus of these specimens was found to be 7273±856 MPa at temperatures below 100°C. This change marks 21% decrease from the storage modulus reported for new specimens. It is important to note that the decrease in the storage modulus is accompanied by an increase in the loss modulus at temperatures below 100°C. Therefore, the complex modulus of the field-deployed and new panel remains the same within the experimental error. Additionally, the T_β transition is present at ~75°C but it is more distinct than beta transition in the new samples. That is, the chain sliding relaxation mechanism is more evident in the field-deployed samples. This, in turn, translates to significant increase in the resilience and toughness of the laminate. Since, T_β for new and old panels remained 75°C, it shows that the chemical composition of the laminate was not altered by the power-line explosion and associated fire. Figure 15 also shows slight change in T_g, which shifted to ~120°C at low frequency and to 127°C at high frequency. The shift in the T_g can be attributed to the change in the stiffness of the surface layer, which was observed by AFM scans.

Numerical Simulation

In addition to the experimental investigation, a finite element analysis (FEA) simulation has been created to simulate the direct impact of the E-glass/Vinyl Ester composite panel by a wire-splice

cover. The cover was modeled as cylindrical projectile made of polyethylene with the following material properties: E = 0.9 GPa, mass density = 958 kg/m^3, ν = 0.49, and strength = 23 MPa. Polyethylene was selected since it is commonly used in electrical insulation. Nonetheless, these properties are common for many types of polymers that are used in the same application. The composite panel was modeled as homogenized laminate that is constructed of 6 layers of E-glass with total skin thickness of 6.55 mm and 13.9 mm thick balsa wood core with stacking sequence of [0_6/Balsa/0_6]. The E-glass laminae and the balsa wood core were modeled as 2D orthotropic materials. The specifications of E-glass ply are: E_1 = 23.4 GPa, E_2 = 9.97 GPa, G_{12} = 3.5 GPa, mass density = 1650 kg/m^3, ν_{12} = 0.28, longitudinal tensile strength = 384 MPa, longitudinal compressive strength = 444 MPa, transverse tensile strength = 164 MPa, transverse compressive strength = 189 MPa, and shear strength = 66.5 MPa [35]. The balsa wood core was assigned the following material properties: E_1 = 4.38 GPa, E_2 = 79 MPa, G_{12} = 189 MPa, mass density = 155 kg/m^3, ν_{12} = 0.488, longitudinal tensile strength = 12.6 MPa, longitudinal compressive strength = 14.1 MPa, transverse tensile strength = 0.8 MPa, transverse compressive strength = 7.5 MPa, and shear strength = 3.1 MPa [35]. The numerical simulation consisted of 10651 quadrilaterals elements, where the composite laminate was meshed using shell elements and the projectile was meshed using solid elements. Figure 16 shows schematics of the numerical model geometry and applied boundary conditions. The panel was fixed ($\bar{u} = 0$) in x- and y-directions and unconstrained in z-direction.

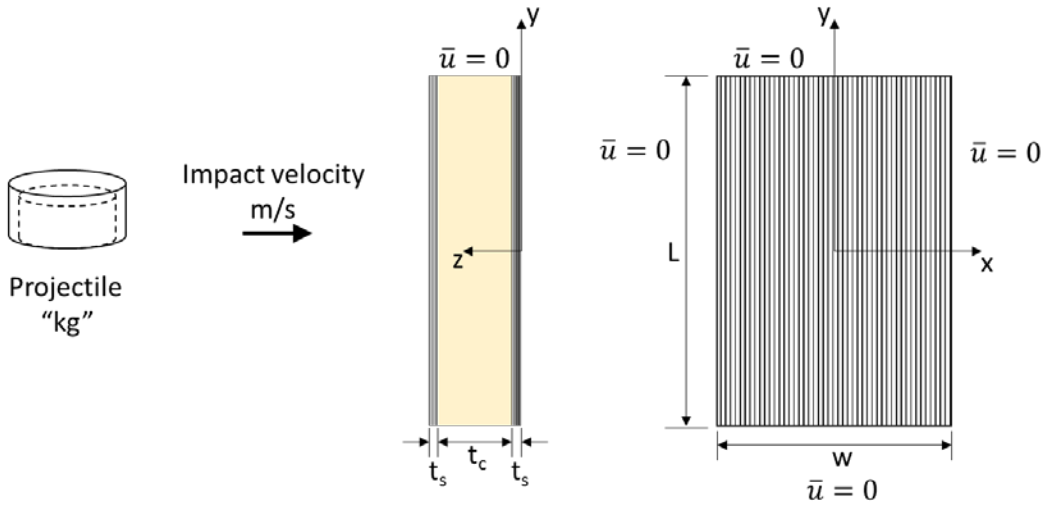

Figure 16: Geometry and boundary conditions of numerical simulation impact study.

The projectile impact velocity was calculated based on the assumption of conservation of energy, the details of which are discussed next. The electric power rating of the vault under consideration was 34.5kVA, which is assumed to have a unity power factor for worst-case energy calculation. The electrical energy ($E_{electrical}$) is then converted to mechanical energy ($E_{mechanical}$), Equation 5, which in turn is used to detach the projectile (splice cover) from the wire assembly ($E_{separation}$), e.g. energy required to separate the wire cover from the wire assembly, and kinetic energy ($E_{kinetic}$).

$$E_{electrical} = E_{mechanical} = E_{separation} + E_{kinetic} \quad (5)$$

The separation energy is based on the bonding strength of the glue used to attach the cover to the wire assembly as well as the bonding area. Figure 17 illustrate cross-sectional view of the assumed geometry of the wire cover and the wire assembly.

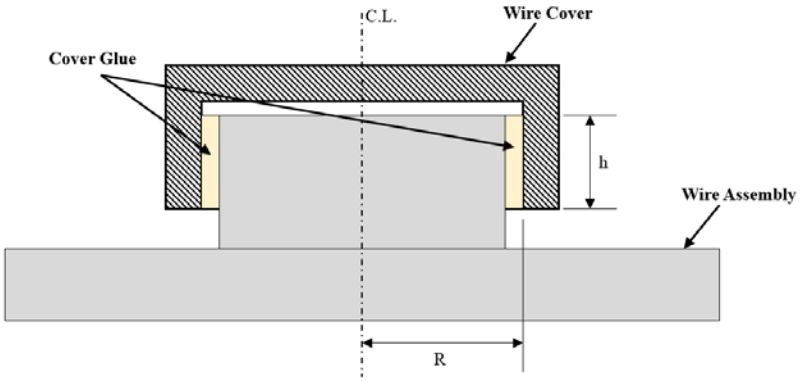

Figure 17: Illustration of assumed cross-sectional view of the glued wire cover and wire assembly.

If the glue shear strength is given as **τ**, therefore the force required to cause adhesive failure at the cover/glue interface

$$F_{af} = \tau . 2\pi Rh \quad (6)$$

where, **R** is the radius of the cover/glue interface, and **h** is the adhesive depth. Thus, the energy required to move the cover h distance is calculated using Eqn.8.

$$E_{separation} = F_{af} . h \quad (7)$$

Meanwhile, the kinetic energy is related the mass of the cover (**m**) and the velocity (**v**) at which the cover will travel.

$$E_{kinetic} = \frac{1}{2} mv^2 \quad (8)$$

The preceding discussion was used to calculate a projectile velocity of ~80 m/s. The impact velocity in the simulation was increased by a factor of 10 since the temperature effect was not taken into account. It is important to note that the calculation of the projectile velocity is based on the absolute worst-case scenario; actual scenarios may vary based on the details of the energy balance. For example in the aforementioned calculation, the energy lost as heat was neglected as well as the potential energy of the cover projectile. Figure 18 shows a screenshot of the velocity calculator, which was designed and included as part of the deliverables package. This calculator can be used to determine the impact velocity, which can be used as an input to the finite element simulation to predict the ply-failure characteristics.

Electric		
Rating	34.5	kVA
Power Factor	1	
P	34.5	kW
t	1	s
$E_{electric}$	34.5	kJ

=

Glue		
τ	0.5	MPa
R	0.2	m
h	0.0762	m
F_{af}	24	kN
$E_{separation}$	2	kJ

+

Kinetic		
m	10	kg
v	81	m/s
$E_{kinetic}$	32.50	kJ

Figure 18: Screenshot of Impact projectile velocity calculator.

Figure 19 shows the maximum principal and shear stresses in each skin ply as well as the transverse tensile, compressive, and shear strengths. The simulation results indicate that the stresses induced due to impact loading are well below the allowable strength of each lamina and thus no ply failure was observed in the FEA simulation. This is consistent with the optical micrographs taken from the field-deployed samples, where no fiber failure was observed.

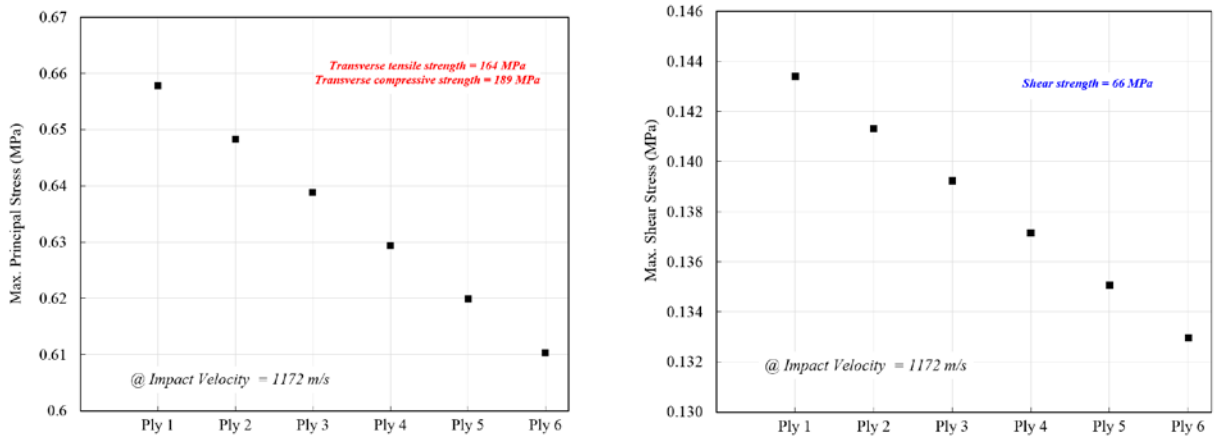

Figure 19: Maximum principal and shear stresses in each ply.

Conclusion

In summary, specimens prepared from new and field-deployed composite panels were experimentally investigated using optical microscope, atomic force microscope, and dynamic mechanical analyzer. These methods provided qualitative and quantitative results to assess the effect of the power-line explosion and in-service conditions on the mechanical performance of the panels. It was found that the burn marks were limited to the surface and were associated with regions where surface contaminates are present. There were no signs of E-glass fiber-failure, inter-laminar failure, skin/core interface failure, or wood fiber failure as shown by the comparison of the micrographs from new and field-deployed samples. The results were also confirmed by numerical simulation, where the induced stresses based on impact and thermal loading were well below the allowable strength of the E-glass lamina and balsa wood core. The burn marks created by the fire produced by the power-line explosion resulted in slight change in the surface stiffness as was demonstrated by the qualitative change in the contrast of AFM phase images. The dynamic mechanical properties of the panels were characterized using DMA in dual-cantilever beam configuration, which simulated in-service loading scenarios. It was found that the worst-case fire-affected specimens exhibited decrease in the storage modulus, while the loss modulus was reported higher than the new samples at temperatures below 100°C. That is, the complex modulus remained unchanged within the experimental error. The overall results indicate that the reported changes are attributed to the changes in the molecular relaxation mechanisms of the matrix phase of the composite panels (i.e., Vinyl Ester) panels while there is no noticeable change to the reinforcement phase (i.e., the fiber). That is, the fiberglass reinforcement did not show any signs of damage as a result of the 34.5kVA power-line explosion. Additionally, the overall results indicated that the fire-retardant properties of the composite panels were effective in mitigating the effect of fire in absence of dust and oil surface contamination. It is then advisable to ensure that the field-deployed composite panels are free of surface contamination for optimal performance.

References:

[1] Karamardian, Vahe, and Aram Stepanian. "Underground utility vault replacement system." U.S. Patent No. 8,307,604. 13 Nov. 2012.
[2] Chun, Lu, and K. Y. Lam. "Dynamic response of fully-clamped laminated composite plates subjected to low-velocity impact of a mass." International journal of solids and structures 35.11 (1998): 963-979.
[3] Shokrieh, Mahmood M., Mohammad A. Torabizadeh, and Abdolhossein Fereidoon. "Dynamic failure behavior of glass/epoxy composites under low temperature using Charpy impact test method." Indian Journal of Engineering & Materials Sciences 18.3 (2011): 211-220.
[4] Mathivanan, N. Rajesh, and J. Jerald. "Experimental Investigation of Woven E-Glass Epoxy Composite Laminates subjected to low-velocity impact at different energy levels." Journal of Minerals and Materials Characterization and Engineering 9 (2010): 643.
[5] Keršys, Artūras, Neringa Keršienė, and Antanas Žiliukas. "Experimental Research of the Impact Response of E-Glass/Epoxy and carbon/Epoxy composite systems." Mater Sci 16.4 (2010): 1392-1320.
[6] Aslan, Züleyha, Ramazan Karakuzu, and Buket Okutan. "The response of laminated composite plates under low-velocity impact loading." Composite Structures 59.1 (2003): 119-127.
[7] Mili, F., and B. Necib. "Impact behavior of cross-ply laminated composite plates under low velocities." Composite structures 51.3 (2001): 237-244.
[8] Richardson, M. O. W., and M. J. Wisheart. "Review of low-velocity impact properties of composite materials." Composites Part A: Applied Science and Manufacturing 27.12 (1996): 1123-1131.
[10] Daniel, Isaac M., et al. Engineering mechanics of composite materials. Vol. 3. New York: Oxford university press, 1994.
[11] Jones, Robert M. Mechanics of composite materials. Vol. 1. New York: McGraw-Hill, 1975.
[12] Christensen, Richard M. Mechanics of composite materials. Courier Corporation, 2012.
[13] Kaw, Autar K. Mechanics of composite materials. CRC press, 2010.
[10] Im, Kwang-Hee, et al. "Effects of temperature on impact damages in CFRP composite laminates." Composites Part B: Engineering 32.8 (2001): 669-682.
[11] Sauerbrunn, S., and P. Gill. "Decomposition kinetics using TGA." American Laboratory 26 (1994): 29-29.
[12] Bin Wadud, S. “improvement in DMA measurements using low-friction 3-point bending clamps.” TA Instruments.
[13] John D. Ferry, Viscoelastic Properties of Polymers – Second Edition. New York: John Willey & Sons Ltd, 1970.
[14] Lawrence E. Nielsen and Robert Landel, Mechanical Properties of Polymers and Composites – Second Edition. New York: Marcel Dekker Inc., 1994.
[15] Wiltold Brostow, Performance of Plastics. Munich: Hanser, 2000.
[16] Thermosets and Composites: Technical Information for Plastics Users, Michel Biron, Elsevier, New York, 2004.
[17] Dynamic Mechanical Analysis: A Practical Introduction, 2nd Edition, Kevin Menard, CRC Press, 2008.
[18] Thermal Characterization of Polymeric Materials – 2nd Ed., Edith Turi, Editor, Academic Press, 1997.
[19] Handbook of Plastics Testing Technology, Vishu Shah, Wiley, New York, 1984.

[20] Handbook of Polymer Analysis, Hubert Lobo and Jose Bonilla, Editors, Dekker, 2003.
[21] Introduction to Polymer Viscoelasticity, Montgomery Shaw and, William J. MacKnight, Wiley, New York, 2005.
[22] Performance of Plastics, Witold Brostow, Editor, Hanser, 2001.
[23] Dynamic Mechanical Analysis for Plastic Engineering, Plastic Design Library, M. Sepe, New York (1998).
[24] T. Murayama, Dynamic Mechanical Analysis of Polymeric Materials, Elsevier, New York (1977).
[25] The Dynamics of Polymer Chains, M. Doi, S. Edwards, Oxford University Press, New York (1986).
[26] Aklonis, Knight, Introduction to Viscoelasticity, Wiley, New York (1983).
[27] Anelastic and Dielectric Effects in Polymer Solids, N. G. McCrum, B. E. Read and G. Williams, Dover, New York, 1967.
[28] Effect of Saline on Epoxy Resin Paint Run in Tension Geometry, PerkinElmer, Application Note 007771A_07, p1-2.
[29] Tg and Cure of a Composite Material, PerkinElmer, Application Note 007771A_08, p1-2.
[30] α and β Relaxations of PMMA and Calculation of the Activation Energy, Application Note 007771A_17, p1-2.
[31] α and β Relaxations of PVC and Calculation of the Activation Energy of the β Event, Application Note 007771A_06, p1-2.
[32] Magonov, S. N., V. Elings, and M-H. Whangbo. "Phase imaging and stiffness in tapping-mode atomic force microscopy." Surface Science 375.2 (1997): L385-L391.
[33] S.N. Magonov, Studies of Polymer Surfaces with Atomic Force Microscopy, Application Note. Digital Instruments, Santa Barbara, CA (October 1995).
[34] ASTM Standard D30.04, 2015, Standard Test Method for Flexural Properties of Polymer Matrix Composite Materials," ASTM International, West Conshohocken, PA, www.astm.org.
[35] Vahe Karamardian, "Material Datasheets used in productions of Voltek panels," Internal communication.

Exhibit 1

Los Angeles Department of Water and Power

Incident Report

34.5 KV Cable Explosion

9401 Oakdale Ave

Northridge, California

Incident Details

Log Item

Address: 9401 OAKDALE AVE BLDG8 6214-0
Start Date: 10/30/14 19:27
Clues: FIX - FIRE \ TRANSFORMER

Area: Valley
District: GH
Duration: 10 hrs 58 minutes

Outage: Yes
Device: RSJ-NR_PED_2
Device Type: RSCIR
Location:
Community: NORTHRIDGE
Estimated: 10/31/14 03:27
Restored: 10/31/14 06:25
Completed: 10/31/14 06:25

Calls: 20
Cust Affected: 142
Critical: 6

DCN:

Device	Calls	Customers	kVA	Start Date	End Date	Lead
RSJ-NR_PED_2	14	142	41250	10/30 19:27	10/31 06:25	T
RSJ-NR_PED_2	6	127	34250	10/30 19:55	10/31 06:25	F

Cause: UNDERGROUND FAULT
Occurrence: 34-5KV\CKT\RELAYED OUT
34-5KV\IS\POTHEAD TROUBLE

Weather: No Description Available for climatic code:

Remarks: 1927 HRS THE NR PED 2 RELAYED AND RECLOSED, SAME TIME NR-PLU 2 RELAYED OUT. CONNECTORS FAILED IN IS-1069 LOC: 9401 OAKDALE AV. TBL ISOLATED VIA FLD SWITCHING AND OPENING DJ-7113 IN MH 9401 OAKDALE AV. 0645 HRS ALL LOAD (EXCEPT IS-1069) PICKED UP VIA FLD SWITCHING. IS-1069 REMAINS OUT DUE TO DAMAGED CABLE AND LID^S. TURNED OVER TO STA MAINT FOR REPAIRS. SEE LOAD DISPATCHERS REPORT FOR FURTHER INFO.

Crew: 187R - BARNES, WILLIAM
Outcome: ASSIST CREW
Assigned: 10/31/14 01:00
Dispatch: 10/31/14 01:01
Arrival: 10/31/14 01:01

Dispatcher: WSOLOMON

Completed: 10/31/14 06:40
Remarks: ASSISTED WITH 34.5 LOCK OUTS.

Crew: 857Y - BUCHANAN, LAWRENCE **Dispatcher:** WSOLOMON
Outcome: ASSIST CREW
Assigned: 10/31/14 07:03
Dispatch: 10/31/14 09:52
Arrival: 10/31/14 09:52
Completed: 10/31/14 19:03
Remarks:

Crew: 885Y - SMISSEN, TED **Dispatcher:** WSOLOMON
Outcome: ASSIST CREW
Assigned: 10/30/14 22:33
Dispatch: 10/30/14 22:33
Arrival: 10/31/14 00:17
Completed: 10/31/14 06:19
Remarks: ASSIST MC GUIRE B.O. CABLE 34.5

Crew: 895Y - MCGUIRE, MICHAEL **Dispatcher:** WSOLOMON
Outcome: OK TEMP
Assigned: 10/31/14 21:00
Dispatch:
Arrival:
Completed: 10/31/14 21:00
Remarks: CKT NR/PED 2 RELAYED OUT @19.49 SWITCHED OUT CKT AS PER LD REQUEST. @DJ 7113 LOC 9401 OAKDALE AVE REMOVED 1/0 AL CLP LATERAL TO IS 1069.(BURNT UP OUTSIDE NR/PLUMMER 1 LID CABINET @ IS1069) ISSUED CLEARANCES TO ESM & DISTRICT SPLICING CREWS TO MAKE PERM REPAIRS.

Crew: 895Y - **Dispatcher:** WSOLOMON
Outcome: OK TEMP
Assigned: 10/30/14 19:35
Dispatch: 10/30/14 19:58

Arrival: 10/31/14 06:41

Completed: 10/31/14 21:00

Remarks: CKT NR/PED 2 RELAYED OUT @19.49 SWITCHED OUT CKT AS PER LD REQUEST. @DJ 7113 LOC 9401 OAKDALE AVE REMOVED 1/0 AL CLP LATERAL TO IS 1069.(BURNT UP OUTSIDE NR/PLUMMER 1 LID CABINET @ IS1069) ISSUED CLEARANCES TO ESM & DISTRICT SPLICING CREWS TO MAKE PERM REPAIRS.

Crew: 896Y - STAUDINGER, JOSHUA **Dispatcher:** WSOLOMON

Outcome: ASSIST CREW

Assigned: 10/30/14 20:10

Dispatch: 10/31/14 00:06

Arrival: 10/31/14 07:01

Completed: 10/31/14 07:02

Remarks: ASSIST CREW 895Y

Crew: 896Y - STAUDINGER, JOSHUA **Dispatcher:** WSOLOMON

Outcome: ASSIST CREW

Assigned: 10/30/14 19:40

Dispatch: 10/30/14 19:46

Arrival: 10/31/14 00:07

Completed: 10/31/14 07:01

Remarks: ASSIST CREW 895Y

Memo(s):

Show: Calls Customers Devices IVR Callbacks Log

1 to 20 of 20

Calls

Device	Address	Clues	Call Date	Operator
IS1069-01	9401 OAKDALE AV	VTS	10/30/14 20:07	KVARGAS
IS2849-01	8810 TAMPA AVE	LO	10/30/14 19:51	DGORD2
IS2142-01	20001 PRAIRIE ST # A	LO	10/30/14 21:29	JMURIL
IS2284-01	20000 PRAIRIE ST	LO	10/30/14 20:46	SVC_IVR
IS2335-01	19867 PRAIRIE ST	LO	10/30/14 20:44	JMURIL
IS2253-01	19850 PLUMMER ST	LO	10/30/14 20:40	PWEINR
RSJ-NR_PED_2	19821 NORDHOFF PL STE 115	LO	10/30/14 19:41	KRENTE

IS1784-01	9046 TAMPA AVE	LO	10/30/14 20:18	PWEINR
NR PED 2 J-4710-01 #2	9222 CORBIN AVE	LO	10/30/14 20:12	PWEINR
IS3437-01	19749 DEARBORN ST	LO	10/30/14 20:10	XBORTIZ
IS3435-01	19350 NORDHOFF ST UNIT C	LO	10/30/14 20:09	PWEINR
IS2142-01	20001 PRAIRIE ST	LO	10/30/14 22:26	SVC_IVR
IS1069-01	9401 OAKDALE AVE BLDG8 6214-0	FIX	10/30/14 20:17	MOGRAD
IS2653-01	9121 OAKDALE AVE	PWO	10/30/14 19:50	SSMIT4
IS1784-01	9040 TAMPA AVE	PWO	10/30/14 20:39	MOGRAD
RSJ-NR_PED_2	8850 TAMPA AVE STE 101	PWO	10/30/14 20:28	MOGRAD
NCC-599	8810 TAMPA AVE	PWO	10/30/14 20:23	PJU
NCC-598	19350 NORDHOFF ST UNIT A	PWO	10/30/14 20:20	MOGRAD
NR-CHA 2 3-Way-3435-01	19350 NORDHOFF ST # C-2	PWO	10/30/14 19:55	IRIOS
RSJ-NR_PED_2	9401 OAKDALE AV	RLS3	10/30/14 19:27	CMACK

Related Links

Update Incident (login required) No attached files exist for this incident.

Incident Search Results

1 to 7 of 7 | ☑Show All

Device	Address / Location	Community	Dist	Calls	Clues	Crew	Job Date	Dispatcher
138-10-089	9521 OAKDALE AVE	CHATSWORTH	GH	1	SVL	893Y	10/15/14 09:48	CMACK
065-16-127	5819 OAKDALE AVE	WOODLAND HILLS	CP	1	LO	854Y	10/16/14 09:40	KVARGAS
RSJ-NR_PED_2	9401 OAKDALE AVE BLDG8 6214-0	NORTHRIDGE	GH	20	FIX	895Y	10/30/14 19:27	WSOLOMON
074-16 S.4	8343 OAKDALE AVE	WINNETKA	GH	3	LF	896Y	10/31/14 16:20	CTWEED
065-14-008	5237 OAKDALE AVE	WOODLAND HILLS	CP	1	LP	854Y	11/12/14 09:22	VGUTIERR
063-23-060	8742 OAKDALE AVE	NORTHRIDGE	GH	1	SVL	187R	11/24/14 10:22	RFLORES
065-16-135	6055 OAKDALE AVE	WOODLAND HILLS	CP	1	LP	894Y	11/26/14 09:08	KVARGAS

Modify your search

1 to 7 of 7

Display Detailed Report On All Results

Distribution Operations Load Dispatching

Circuit Interruptions

From 2/23/2014 to 3/2/2015

Interrupt No	Circuit Name	Date	Time	Cause	RS	Section
9424	NR PED 2	10/30/2014	1948	Connectors failed in MH-9401 Oakdale Ave. and in Vault 19900 Prairie St.	J	A
9422	NR PED 2	10/30/2014	1927	Connectors failed in MH-9401 Oakdale Ave. and in Vault 19900 Prairie St.	J	A
9386	NR PED 2	9/10/2014	352	The cause has not been determined	J	A